8-1-1991

Gravity Wave-Driven Fluctuations in OH Nightglow from an Extended, Dissipative Emission Region

G. Schubert
Institute of Geophysics and Planetary Physics, University of California

R. L. Walterscheid
The Aerospace Corporation

Michael P. Hickey Ph.D.
Embry-Riddle Aeronautical University, hicke0b5@erau.edu

Scholarly Commons Citation

Schubert, G., R. L. Walterscheid, and M. P. Hickey (1991), Gravity wave-driven fluctuations in OH nightglow from an extended, dissipative emission region, J. Geophys. Res., 96(A8), 13869–13880, doi: https://doi.org/10.1029/91JA00562

JOURNAL OF GEOPHYSICAL RESEARCH, VOL. 96, NO. A8, PAGES 13,869–13,880, AUGUST 1, 1991

Gravity Wave-Driven Fluctuations in OH Nightglow From an Extended, Dissipative Emission Region

G. SCHUBERT AND R. L. WALTERSCHEID

Space Sciences Laboratory, The Aerospace Corporation, Los Angeles, California

M. P. HICKEY[1]

Universities Space Research Association, NASA Marshall Space Flight Center, Huntsville, Alabama

The theory of gravity wave-driven fluctuations in the OH nightglow from an extended source region is generalized to account for effects of eddy kinematic viscosity ν and eddy thermal diffusivity κ. In the nondiffusive case, the amplitudes and phases of vertically integrated normalized intensity $\langle \delta I \rangle / \langle \bar{I} \rangle$ and temperature $\langle \delta T_I \rangle / \langle \bar{T}_I \rangle$ perturbations and vertically integrated Krassovsky's ratio $\langle \eta \rangle$ as functions of period are influenced by the upper limit of vertical integration of the extended source, especially at long periods when vertical wavelengths λ_v are small. The effects, which include oscillations in $\langle \delta T \rangle / \langle \bar{I} \rangle$, $\langle \delta T_I \rangle / \langle \bar{T}_I \rangle$, and $\langle \eta \rangle$, particularly at long periods, are due to constructive and destructive interference of nightglow signals from vertically separated levels of the OH emitting region that occur when λ_v is comparable to or smaller than the thickness of the main emission region. The sensitivity of these ratios to the upper limit of vertical integration occurs because of the relatively small rate of decay of the intensity of OH emission with height above the peak emission level and the exponential growth with altitude of nondissipative gravity waves. Because eddy diffusion increases λ_v, especially at long periods, and reduces wave growth with height compared with the case $\nu = \kappa = 0$, inclusion of eddy diffusion removes the sensitivity of $\langle \eta \rangle$ and the other ratios to the maximum height of vertical integration. It is essential to account for both eddy diffusion and emission from the entire vertically extended emission region to correctly predict $\langle \eta \rangle$, $\langle \delta I \rangle / \langle \bar{I} \rangle$, and $\langle \delta T_I \rangle / \langle \bar{T}_I \rangle$ at long gravity wave periods. Observations of Krassovsky's ratio are consistent with theoretical predictions of $\langle \eta \rangle$ for horizontal wavelengths larger than about 500 km, provided diffusion and emission from an extended region are both taken into account.

INTRODUCTION

It is now widely accepted that acoustic-gravity waves and tides modulate the intensity of the hydroxyl (OH) nightglow by upsetting the OH chemical equilibrium around the mesopause, the approximate region of peak OH emission. The theoretical modeling of the chemical and dynamical processes involved in this modulation has been the subject of much study, but it is only the most recent analyses that have been able to account for some of the observed features of the measured oscillations. A principal objective of these analyses has been the calculation of the parameter η [*Krassovsky*, 1972], which relates the oscillation in the intensity (δI) of the nightglow to the oscillation in the temperature (δT) of the emission region by $\eta = (\delta I/\bar{I})/(\delta T/\bar{T})$, where an overbar refers to the undisturbed or time-averaged variable. *Walterscheid et al.* [1987] calculated η using a model that incorporates the Eulerian dynamics of linearized acoustic-gravity waves and the chemistry of the five minor species O, O_3, H, OH, and HO_2 controlling the concentration of excited OH. The ability of the model to explain observed oscillations in the nightglow intensity and emission region temperature was subsequently demonstrated by *Hecht et al.* [1987] and *Sivjee et al.* [1987]. *Walterscheid and Schubert* [1987] generalized the model to deal with OH nightglow fluctuations induced by tides.

The above definition of Krassovsky's ratio and the theory of *Walterscheid et al.* [1987] and *Walterscheid and Schubert* [1987] pertain to an infinitesimally thin nightglow emission layer. The importance of considering the nonzero vertical extent of the emission region in the calculation and interpretation of Krassovsky's ratio has been demonstrated by *Hines and Tarasick* [1987] and *Schubert and Walterscheid* [1988]. Interference effects modify the intensity, the intensity-weighted temperature, and Krassovsky's ratio for waves having vertical wavelengths less than or comparable to the main emission layer thickness and, as we show later, are sensitive to the assumed height of the upper boundary of the emission region.

The thin-layer model of *Walterscheid et al.* [1987] was modified by *Hickey* [1988*a*, *b*] to include effects of eddy momentum and thermal diffusivities on gravity wave dynamics. These effects substantially influence the value of Krassovsky's ratio at long gravity wave periods. The observations of *Viereck and Deehr* [1989] suggest that the effects of eddy kinematic viscosity and eddy thermal diffusivity are discernible in the OH nightglow fluctuations.

The purpose of the present paper is to investigate how the characteristics of the OH nightglow from an extended emission region are modified by eddy momentum and eddy thermal diffusivities. This generalization of the theory of *Schubert and Walterscheid* [1988] is important not only for the purpose of completing the theory but also because the effects of eddy kinematic viscosity and eddy thermal diffusivity are expected to be significant for nightglow fluctuations induced by gravity waves with small vertical wavelengths [*Hickey*, 1988*a*, *b*]; these are precisely the waves

[1]Now at FWG Associates, Huntsville, Alabama.

Paper number 91JA00562.
0148-0227/91/91JA-00562$05.00

whose induced nightglow fluctuations are most affected by interference effects associated with the finite altitude of the top of the emission layer.

THEORY

We follow closely the approach of *Schubert and Walterscheid* [1988] but extend their model to incorporate effects of eddy kinematic viscosity and eddy thermal diffusivity. The atmosphere consists of a major gas (N_2 + O_2) and the minor species OH, H, O_3, O, and HO_2. The number densities n of the atmospheric constituents and the temperature T of the atmosphere are determined by contributions from a time-independent basic state (denoted by an overbar) and wave-driven fluctuations (denoted by δ). The nighttime model atmosphere of *Winick* [1983] is adopted for the basic state. Minor constituent chemistry and reaction rates, as well as a detailed description of the basic state, are given by *Schubert and Walterscheid* [1988].

Reactions between H and O_3 and between O and HO_2 yield excited OH molecules that subsequently decay and produce the nightglow. Ground-based spectrophotometric observations of the nightglow record a vertically integrated intensity $\langle I\rangle = \langle \bar{I}\rangle + \langle \delta I\rangle$ (angle brackets denote integration over the height of the emission region). The intensity fluctuations $\langle \delta I\rangle$ are caused by gravity wave-driven fluctuations in n and T. Temperatures inferred from ground-based spectrophotometric observations of the OH nightglow are intensity weighted according to

$$\langle T_I\rangle = \int dz\ TI/\langle I\rangle \tag{1}$$

where z is height [*Schubert and Walterscheid*, 1988]. Krassovsky's ratio for a vertically extended emission region is given by

$$\langle \eta\rangle = \frac{\langle \delta I\rangle/\langle \bar{I}\rangle}{\langle \delta T_I\rangle/\langle \bar{T}_I\rangle} \tag{2}$$

[*Schubert and Walterscheid*, 1988]. For the basic state of *Winick* [1983], the peak in OH emission occurs at about 83 km altitude, and the vertical thickness of the main emission region is about 13 km (vertical distance between levels whose intensities are 10% of the peak intensity) [*Schubert and Walterscheid*, 1988].

The formalism for computing $\langle \eta\rangle$ makes use of continuity equations for the number density perturbations δn of the minor species, chemical equations for volumetric production and loss rates of the minor constituents, and dynamical equations relating density, velocity, and temperature perturbations according to acoustic-gravity wave theory. It is assumed that the contribution of an infinitesimal volume to the intensity of the OH nightglow is directly proportional to the volumetric production rate of excited OH. All perturbation quantities are associated with a vertically propagating wave whose amplitude and phase are determined as functions of height by vertically integrating (A10) with the vertical wavenumber given by the isothermal dispersion relation of the appendix evaluated at local conditions. Number density perturbations of minor constituents and their production and loss rates are also calculated with the polarization relations of the appendix evaluated at local conditions. A detailed description of the methodology is given by *Walterscheid et al.* [1987] and *Schubert and Walterscheid* [1988], except for the generalization of acoustic-gravity wave theory to include eddy momentum and eddy thermal diffusivities ν and κ, respectively. This generalization is carried out in the appendix.

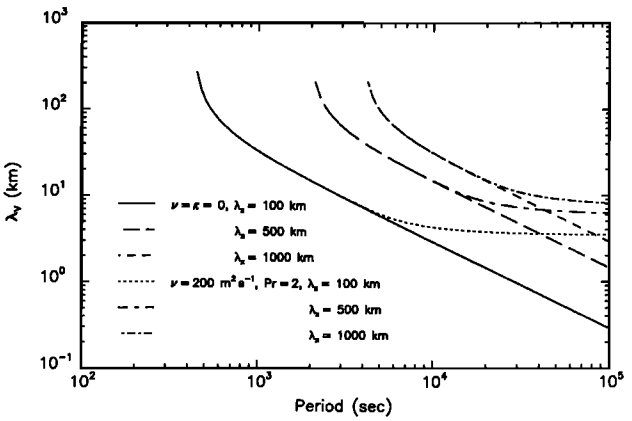

Fig. 1. Vertical wavelength $\lambda_v = 2\pi/\mathrm{Re}(k_z)$ at the peak emission height of about 83 km as a function of period for three different horizontal wavelengths λ_x = 100, 500, and 1000 km. The curves which tend to flatten at long periods include effects of eddy diffusion with ν = 200 m^2 s^{-1} and Pr = 2. The other curves for which λ_v decreases with period as periods become long have no eddy diffusion $\nu = \kappa = 0$.

RESULTS

The model atmosphere (temperature, major and minor gas number densities) is that of *Winick* [1983]. All model parameters are given by *Schubert and Walterscheid* [1988] and *Walterscheid et al.* [1987], except for the values of the eddy momentum diffusivity ν and the eddy thermal diffusivity κ. For nominal values of ν and κ, we adopt 200 and 100 m^2 s^{-1}, respectively, corresponding to an eddy Prandtl number $Pr \equiv \nu/\kappa$ of 2 [*Hickey*, 1988*a*, *b*]. We will investigate the effects of varying ν and κ by considering ν = 50 m^2 s^{-1} with Pr = 2 and ν = 200 m^2 s^{-1} with Pr = 10, a large value for the eddy Prandtl number. Eddy diffusivities are assumed constant with altitude.

The vertical wavelength $\lambda_v = 2\pi/\mathrm{Re}(k_z)$ is the main property of the gravity wave (ω is the circular frequency; k_x is the horizontal wavenumber; λ_x is the horizontal wavelength; and k_z is the complex vertical wavenumber) that determines how OH fluctuations will be affected by eddy diffusivity and emission layer thickness. Wave damping is enhanced as λ_v decreases, while interference effects due to the maximum height of the emission region become more important as λ_v decreases and becomes comparable to and smaller than the main emission layer thickness. Accordingly, in Figure 1 we show λ_v at the peak emission height of about 83 km as a function of period for the nominal values of ν and κ and for λ_x = 100, 500, and 1000 km. In addition, Figure 1 shows λ_v versus period for cases with no diffusion; $\nu = \kappa = 0$. Effects of eddy diffusion cause λ_v to become independent of period as periods tend to large values. With no eddy diffusion, λ_v decreases as periods become large. Eddy diffusion becomes important in limiting the decrease in vertical wavelength with increasing period when λ_v de-

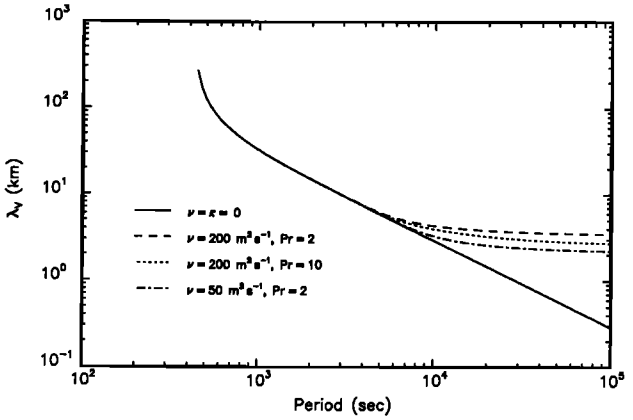

Fig. 2. Similar to Figure 1, but for λ_x = 100 km and for different values of ν and Pr. The case ν = 200 m^2 s^{-1} and Pr = 2 is referred to as the nominal case in the text. The figure illustrates the effects of varying diffusivity values on λ_v versus period.

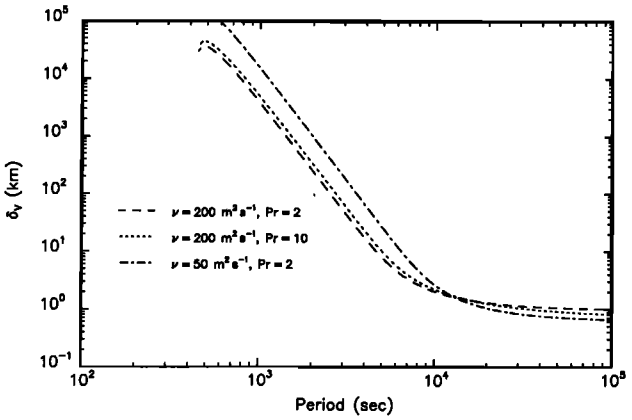

Fig. 4. The influence of different eddy diffusivity parameters on the period dependence of the vertical attenuation distance δ_v at the peak emission height for λ_x = 100 km.

creases to about 10 km (for ν = 200 m^2 s^{-1}, Pr = 2). The vertical wavelength at which effects of eddy diffusion become significant decreases from about 15 to 6 km as the horizontal wavelength decreases from 1000 to 100 km.

Figure 2, for λ_x = 100 km, shows that the effects of eddy diffusion on the vertical wavelength λ_v at the peak emission height are not particularly sensitive to the assumed values of the eddy diffusivities, at least for the variations in ν and κ considered here. Compared with the nominal case, an increase in eddy Prandtl number or a decrease in eddy kinematic viscosity shifts the flattening in the curve of λ_v versus period to larger periods and smaller vertical wavelengths.

The vertical wavenumbers of gravity waves are purely real when $\nu = \kappa = 0$. When eddy diffusive effects become important, the waves are damped, as shown by the vertical attenuation length $\delta_v \equiv 1/\text{Im}\ (k_z)$ at the peak emission height plotted in Figure 3 as a function of period for the nominal set of diffusivity parameters and for λ_x = 100, 500, and 1000 km. The vertical attenuation length δ_v decreases with increasing period (except for a very small period interval near the maximum in δ_v) and tends toward a constant value as the period becomes large. The asymptotic value of δ_v decreases from about 3 km for a horizontal wavelength of 1000 km to about 1 km for λ_x = 100 km. Figure 4, for λ_x = 100 km, shows that the value of δ_v at the peak emission height is relatively insensitive to the variations in the eddy diffusion parameters considered here, especially at long periods. The vertical length scale for damping a gravity wave by a factor of e through eddy diffusion tends to about $0.3\lambda_v$ as period increases to large values, independent of the values of λ_x and the diffusivity parameters considered here.

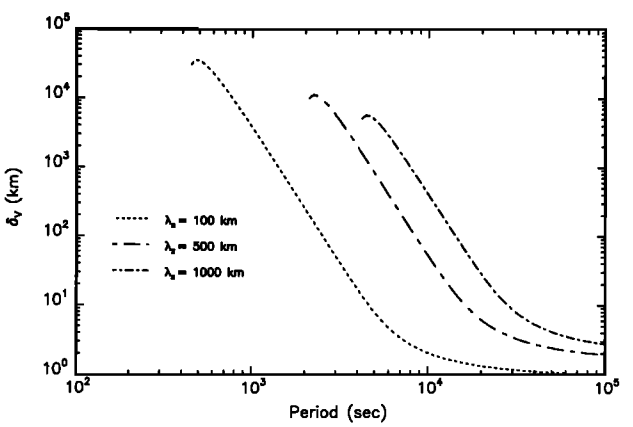

Fig. 3. Vertical attenuation distance $\delta_v = 1/\text{Im}\ (k_z)$ at the peak emission height versus period for λ_x = 100, 500, and 1000 km and for ν = 200 m^2 s^{-1}, Pr = 2. The vertical wavenumber is purely real when $\nu = \kappa = 0$.

The polarization factors f_1, f_2, and f_3, which relate the fluctuations in velocity divergence, vertical velocity, and background density, respectively, to fluctuations in temperature (see the appendix), are shown as functions of period in Figures 5–7 for $\nu = \kappa = 0$ and for the nominal diffusivities with λ_x = 100, 500, and 1000 km. The polarization factors in these figures are evaluated at the peak emission altitude. With $\nu = \kappa = 0$, the amplitude of the velocity divergence factor f_1 decreases monotonically with period ($f_1 \sim$ period^{-1}) (Figure 5*a*), while the phase of f_1 lags the temperature fluctuation by $\pi/2$ (Figure 6); f_1 is independent of λ_x when ν and κ are zero. When ν and κ are nonzero, $|f_1|$ decreases with period, but it approaches a constant as period tends toward large values ($\gtrsim 10^5$ s, Figure 5*a*, for nominal values of ν and κ). In the diffusive case, the asymptotic value of the amplitude of the velocity divergence factor decreases from about 2×10^{-3} s^{-1} at λ_x = 100 km to about 4×10^{-4} at λ_x = 1000 km (Figure 5*a*). In the presence of nonzero eddy diffusivity, the phase of f_1 decreases with increasing period (f_1 lags further behind the temperature fluctuation) and approaches a constant value at very long periods ($\gtrsim 10^5$ s, Figure 5*b*). The phase lag between f_1 and the temperature perturbation decreases with increasing λ_x (Figure 5*b* for the nominal diffusivity values).

The amplitude of the vertical velocity polarization factor f_2 generally decreases with increasing period (Figure 6*a*); the decrease in $|f_2|$ with period is mitigated by nonzero diffusivity ($|f_2|$ tends toward a constant value at long periods, $\gtrsim 10^5$ s, which decreases with increasing λ_x). The phase of f_2 generally lags the phase of the temperature perturbation (Figure 6*b*). With $\nu = \kappa = 0$, the phase of f_2 generally becomes less negative with increasing period, tending to-

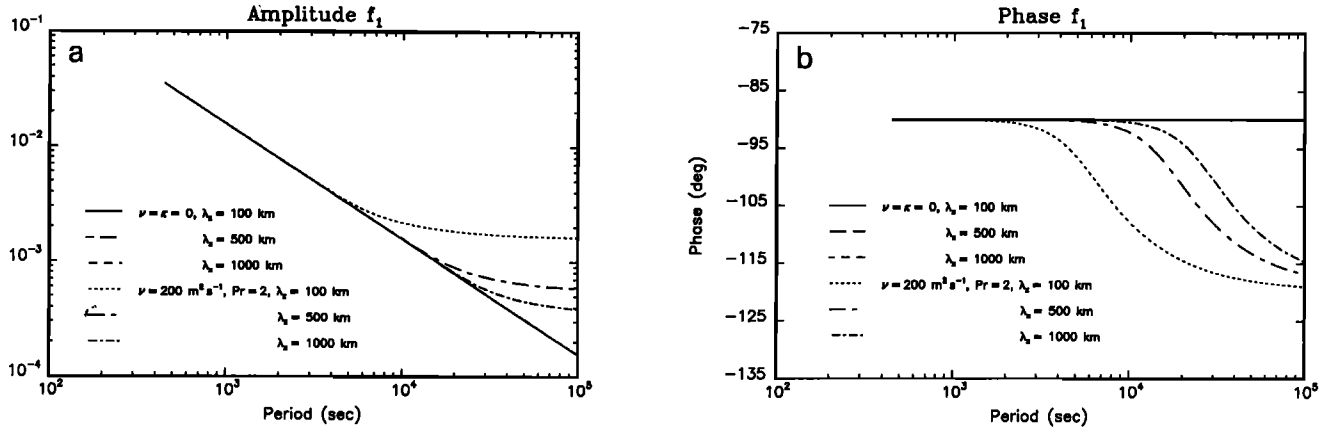

Fig. 5. (*a*) Amplitude and (*b*) phase of the velocity divergence polarization factor f_1 for gravity waves as a function of period for no eddy diffusion and for $\nu = 200$ m^2 s^{-1}, $Pr = 2$ with horizontal wavelength $\lambda_x = 100$, 500, and 1000 km. The polarization factor f_1 relates the velocity divergence fluctuation to the temperature perturbation of the gravity wave; f_1 is evaluated at the peak emission altitude and has units of s^{-1}.

ward $-\pi/2$ at long periods ($\gtrsim 10^5$ s). However, nonzero eddy diffusivity reverses this trend; the phase of f_2 lags further behind the phase of the temperature as period increases.

The magnitude of the background density polarization factor f_3 increases with increasing period toward a constant value that depends on the values of the diffusivity parameters and λ_x (Figure 7*a*). The asymptotic value of $|f_3|$ is somewhat larger for the nominal diffusivity values than it is for $\nu = \kappa = 0$, and with nonzero diffusivity the asymptotic value of $|f_3|$ increases slightly with increasing λ_x. The phase of f_3 generally increases toward π with increasing period when $\nu = \kappa = 0$, while it becomes more negative with increasing period, approaching about $-\pi$ at long periods ($\gtrsim 10^5$ s), for the nominal diffusivity values (Figure 7*b*).

Figures 8–10 show how changes in the eddy diffusivity values affect the dependence of the polarization factors f_1, f_2, and f_3 on period for $\lambda_x = 100$ km. The polarization factors in Figures 8–10 are evaluated at the peak emission altitude. The increase in Pr from 2 to 10 and the decrease in ν from 200 to 50 m^2 s^{-1} both decrease the magnitudes of all the polarization factors and make the phases of the factors less negative (though the phase of f_3 is little affected by the changes in ν and Pr).

The magnitude of the ratio of the height-integrated intensity perturbation to the vertically integrated intensity of the basic state, $\langle \delta I \rangle / \langle \bar{I} \rangle$, is shown in Figure 11 as a function of wave period for $\nu = \kappa = 0$ and for the nominal eddy diffusivities with $\lambda_x = 100$, 500, and 1000 km. Without eddy diffusion, the amplitude of $\langle \delta I \rangle / \langle \bar{I} \rangle$ generally decreases with increasing period, though there are oscillations due to interference effects associated with the finite thickness of the emission region [*Schubert and Walterscheid*, 1988]. These interference effects are important whenever the vertical wavelength of the wave is less than or comparable to the main emission layer thickness. The interference oscillations are different in detail from those of *Schubert and Walterscheid* [1988], since we used a smoother representation of the basic state in the present paper and carried the present vertical integrations to a greater height. Some detailed characteristics of the interference oscillations in this and later figures are due to the finite altitude of the upper limit of the vertical integrations. In this paper the vertical integration range extends between 75 and 120 km (compared with 78–88 km in work by *Schubert and Walterscheid* [1988]). The basic state altitude profiles of *Winick* [1983] for the number densities of H, O_3, HO_2, and OH were linearly extrapolated with altitude above heights of 110, 100, 95, and 95 km, respectively, in order to minimize interference effects. The

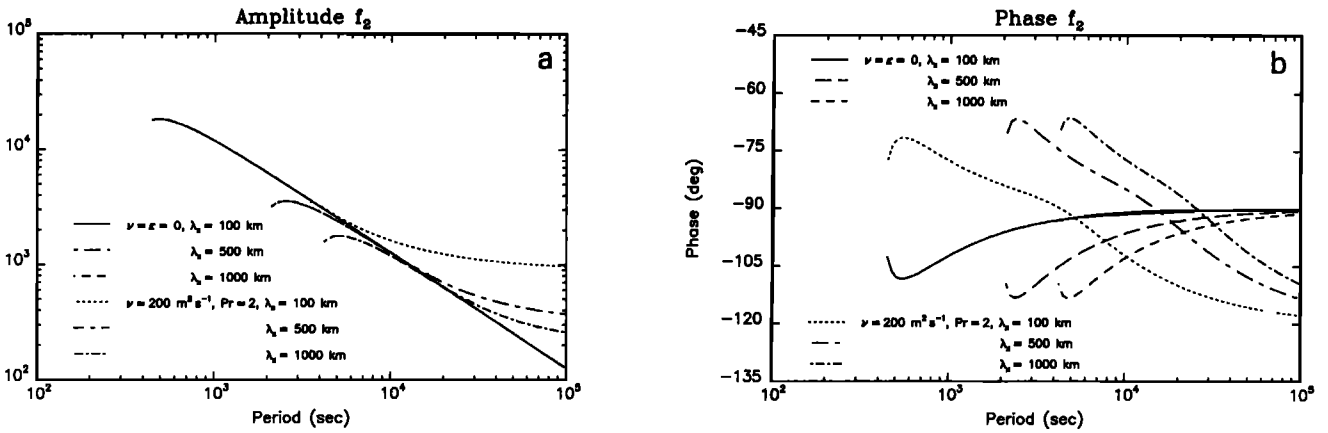

Fig. 6. Similar to Figure 5, but for the vertical velocity polarization factor f_2. The units of f_2 are cm s^{-1}.

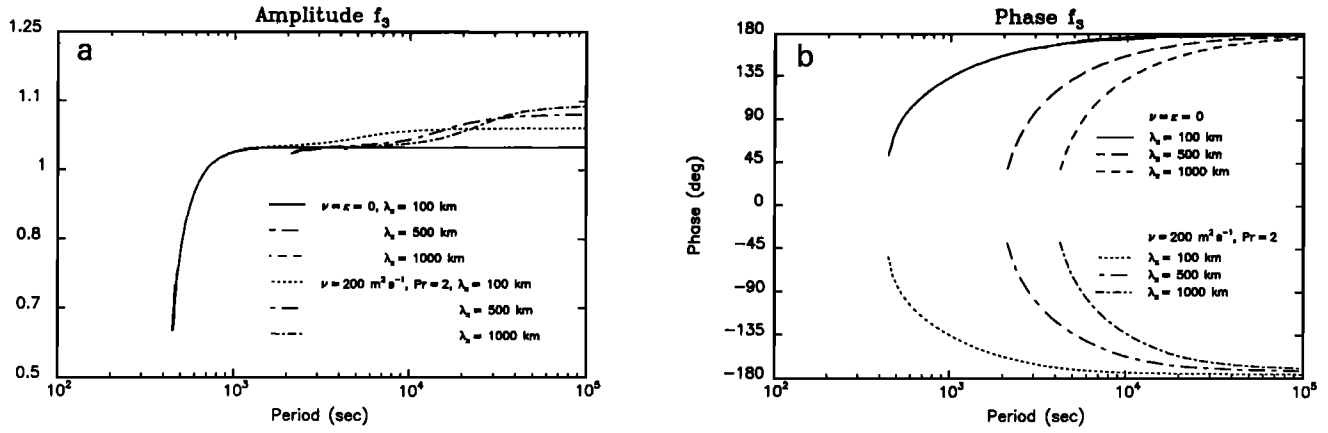

Fig. 7. Similar to Figure 5, but for the background gas density polarization factor f_3.

sensitivity of $\langle \delta I \rangle / \langle \bar{I} \rangle$ (and of the ratios $\langle \delta T_I \rangle / \langle \bar{T}_I \rangle$ and $\langle \eta \rangle$ to be discussed later) to the altitude of the upper limit of vertical integration results from the relatively small rate of decay of the intensity of OH emission with height above the peak emission level [*Schubert and Walterscheid*, 1988] and from the exponential growth of nondissipative gravity waves with height.

A test of the ability of the numerical integration scheme to account for interference effects was performed by comparing numerical results to analytical results for a highly idealized model. We used the analytical solution for Krassovsky's ratio obtained by *Tarasick and Hines* [1990] for the case wherein excited OH is produced only by H reacting with O_3, perturbations in H and O_3 are caused by dynamics alone, and the background atmosphere is isothermal. For λ_x = 1000 km, we find exact agreement between the numerical and analytical solutions for all the periods considered (gravity wave periods up to 10^5 s). For λ_x = 100 km, the solutions agree up to periods of 10^4 s and diverge at longer periods. The numerical results for intensity, temperature, and Krassovsky's ratio as a function of wave period shown in Figures 11, 13, and 15, respectively, exhibit smooth monotonic behavior at short gravity wave periods, followed by slow, fairly regular undulations at longer wave periods. For λ_x = 100 km, this behavior is followed at yet longer periods by irregular or anomalous behavior. The wave period at which this irregular behavior commences agrees with the period at which the numerical and analytical solutions diverge in the simple case discussed above. We conclude that the irregular behavior at long periods is definitely an artifact of the emission layer having finite thickness but that the slower, smoother undulations at intermediate periods may be real interference oscillations resulting from chemistry and a nonisothermal atmosphere. For periods at which interference effects are clearly artifacts, the amplitude of the intensity fluctuation is reduced by several orders of magnitude compared with the intensity amplitude at periods where interference effects are absent.

Because eddy diffusion increases vertical wavelength compared with the nondiffusive case at long gravity wave periods and damps vertically propagating waves, inclusion of eddy diffusion smooths out the interference oscillations in $|\langle \delta I \rangle / \langle \bar{I} \rangle|$ that are associated with the finite vertical thickness of the emission layer. The tendency for λ_v to approach a constant value at large gravity wave periods when eddy diffusion is accounted for (Figure 1) leads to larger values of $|\langle \delta I \rangle / \langle \bar{I} \rangle|$ at these periods, compared to the $\nu = \kappa = 0$ case, even though diffusion tends to reduce wave amplitudes as the waves propagate vertically. By mitigating against interference effects, the inclusion of eddy diffusion also removes

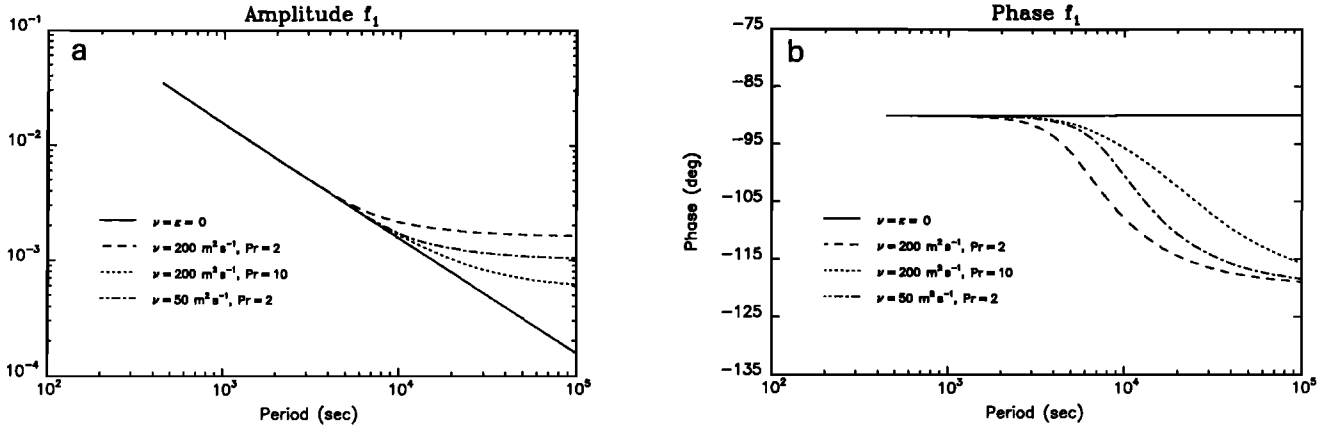

Fig. 8. Effects of varying the diffusivity parameters on the period dependence of the (*a*) amplitude and (*b*) phase of the velocity divergence polarization factor f_1. Horizontal wavelength is 100 km, and f_1 is evaluated at the peak emission height. The units of f_1 are s^{-1}.

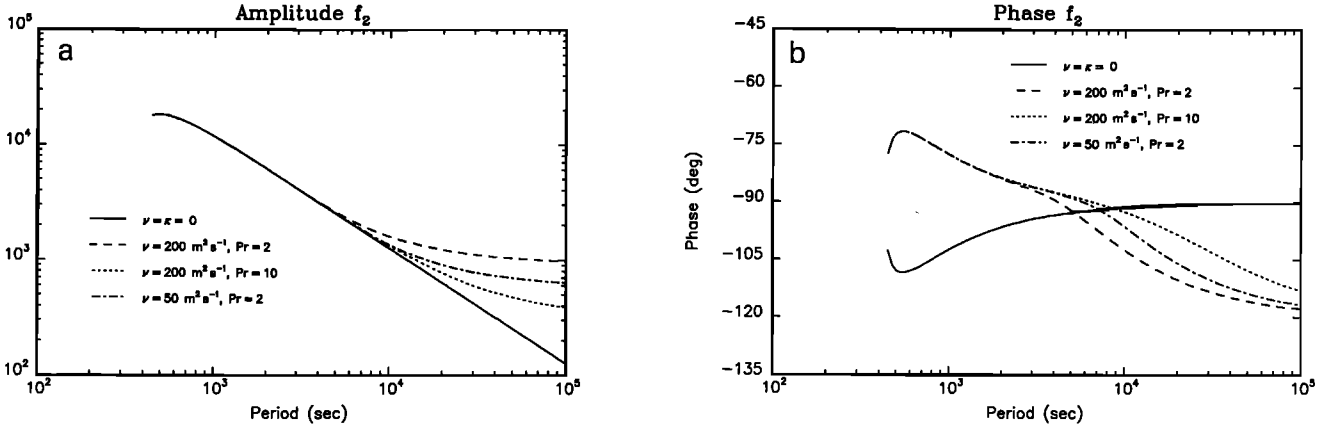

Fig. 9. Similar to Figure 8, but for f_2. The units of f_2 are cm s^{-1}.

the strong oscillatory character (with period) in the phase of $\langle \delta I \rangle / \langle \bar{I} \rangle$.

The influence of variations in the diffusivity parameters on the dependence of $\langle \delta I \rangle / \langle \bar{I} \rangle$ on period is shown in Figure 12 for $\lambda_x = 100$ km. For the diffusivity changes considered here (an increase in Pr with ν held fixed and a decrease in ν with Pr held fixed), $|\langle \delta I \rangle / \langle \bar{I} \rangle|$ is reduced (compared to the nominal diffusive case) at long periods (Figure 12*a*). However, for all the diffusive cases considered, the amplitude of $\langle \delta I \rangle / \langle \bar{I} \rangle$ exceeds that of the nondiffusive case at long periods. The flattening of the curve for $Pr = 2$, $\nu = 50$ m^2 s^{-1} at a period of about 1.5×10^4 s might be an effect of the limited range of the vertical integration. Figure 12*b* shows, for $\lambda_x = 100$ km, how the phase of $\langle \delta I \rangle / \langle \bar{I} \rangle$ is strongly modified and smoothed by the nonzero diffusivities. For example, at periods less than about 10^4 s, nonzero diffusivity changes the sign of the phase, compared to the case $\nu = \kappa = 0$. The interference oscillatory character of the phase at periods greater than 10^4 s for $\nu = \kappa = 0$ completely disappears in the presence of diffusion. The phase of the normalized, height-integrated intensity fluctuation is influenced by the actual values of the eddy diffusivities, especially at periods greater than about 10^4 s.

Figure 13 shows the amplitude of $\langle \delta T_I \rangle / \langle \bar{T}_I \rangle$ versus period for the nondissipative case and for the nominal values of ν and κ when $\lambda_x = 100$, 500, and 1000 km. There is less oscillatory interference structure in $|\langle \delta T_I \rangle / \langle \bar{T}_I \rangle|$ versus period than there is in $|\langle \delta I \rangle / \langle \bar{I} \rangle|$ versus period in the nondiffusive case. The main effect of nonzero diffusivity is to maintain the level of the amplitude of the height-integrated normalized temperature perturbation at long periods compared to the strong decrease with period, at long periods, in the nondiffusive case. The shelf in the curve for $\nu = \kappa = 0$ at a period of about 6×10^3 s might be due to the limited range of the vertical integration.

The effects of changes in the diffusivity parameters on the dependence of $\langle \delta T_I \rangle / \langle \bar{T}_I \rangle$ on period is shown in Figure 14 for $\lambda_x = 100$ km. The increase in Pr and the decrease in ν from their nominal values lead to lower values of $|\langle \delta T_I \rangle / \langle \bar{T}_I \rangle|$, compared to the nominal diffusive case, at periods larger than about 10^4 s (Figure 14*a*). The flattening of the curve for $Pr = 2$, $\nu = 50$ m^2 s^{-1} at a period of about 10^4 s (Figure 14*a*) may be related to the limited range of the vertical integration. The sensitivity of the phase of the normalized height-integrated temperature perturbation to the actual values of ν and κ is emphasized in Figure 14*b*. As was the case for the phase of $\langle \delta I \rangle / \langle \bar{I} \rangle$ versus period, nonzero diffusion changes the sign of the phase of $\langle \delta T_I \rangle / \langle \bar{T}_I \rangle$ at periods less than about 10^4 s compared with the nondiffusive case and smooths out the interference oscillations in the phase of $\langle \delta T_I \rangle / \langle \bar{T}_I \rangle$ compared with the case $\nu = \kappa = 0$ at periods greater than about 10^4 s.

Figure 15 shows the amplitude of the vertically integrated Krassovsky's ratio $\langle \eta \rangle$ as a function of period for the three

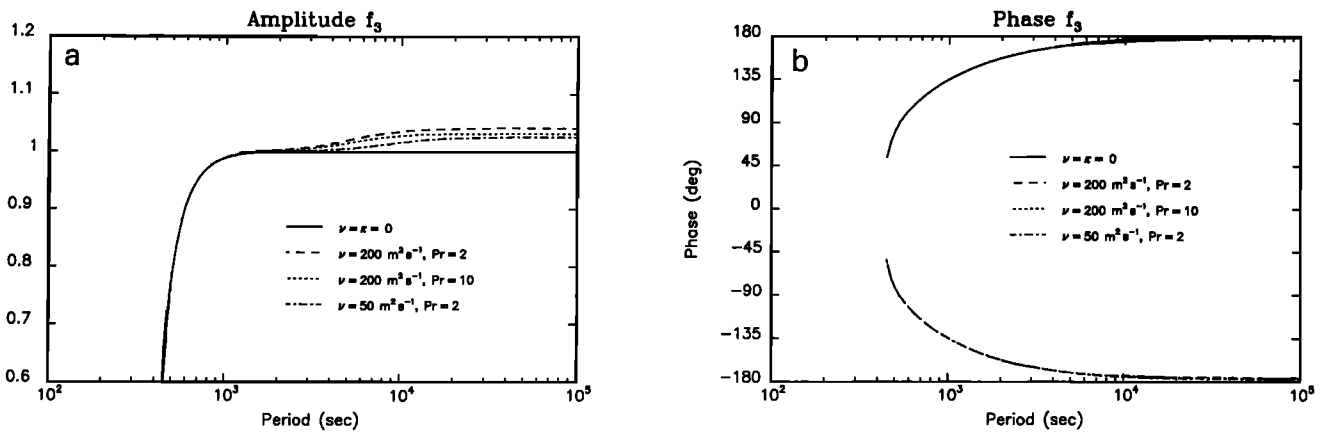

Fig. 10. Similar to Figure 8, but for f_3.

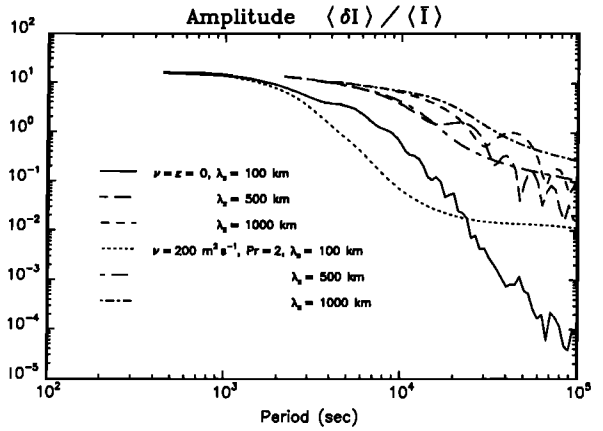

Fig. 11. Amplitude of the vertically integrated normalized intensity perturbation $\langle \delta I \rangle / \langle \bar{I} \rangle$ as a function of period for λ_x = 100, 500, and 1000 km and for $\nu = \kappa = 0$ and for $\nu = 200$ m^2 s^{-1}, $Pr = 2$. The curves for the case $\nu = \kappa = 0$ oscillate as a function of period due to interference effects in emission from an extended layer. Eddy diffusion smooths out the interference oscillations.

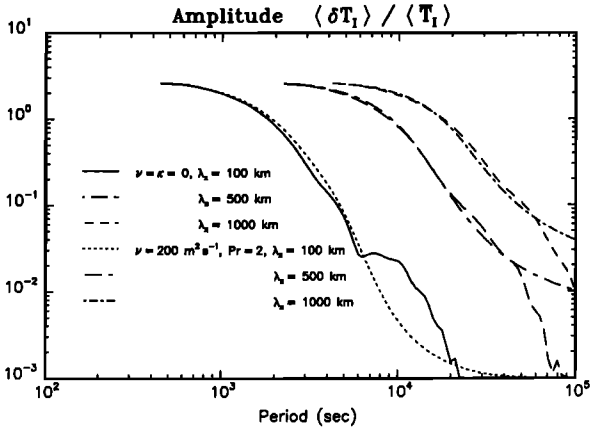

Fig. 13. Similar to Figure 11, but for the height-integrated normalized temperature perturbation $\langle \delta T_I \rangle / \langle \bar{T}_I \rangle$.

values of λ_x considered in the previous figures and for $\nu = \kappa = 0$ and ν and κ equal to their nominal values. The large interference fluctuations that occur in the amplitude of $\langle \eta \rangle$ versus period when $\nu = \kappa = 0$ are removed when eddy diffusion is taken into account. As noted previously, the detailed structures of the interference oscillations in $|\langle \eta \rangle|$ versus period for the nondiffusive cases are different from those of *Schubert and Walterscheid* [1988] because of the sensitivity of interference effects to the value of the upper limit of vertical integration. Even the interference oscillations in Figure 15 are influenced by the higher extent of vertical integration used in this paper. While the diffusive cases in Figure 15 do not have the interference oscillations, the exact form of $|\langle \eta \rangle|$ versus period when ν and κ are nonzero is nevertheless affected by the upper limit of vertical integration. The effect is largest for λ_x = 100 km, which has the smallest vertical wavelength (Figure 1). It is seen from Figure 15 that $|\langle \eta \rangle|$ is insensitive to diffusion for gravity wave periods close to the evanescent region, periods at which the nondiffusive $|\langle \eta \rangle|$ has no interference oscillations; the vertical wavelength is large and independent of diffusion at periods close to the evanescent region (Figure 1).

The way in which different values of ν and κ affect $\langle \eta \rangle$ versus period is illustrated in Figure 16 for λ_x = 100 km. The magnitude (Figure 16*a*) of $\langle \eta \rangle$ is independent of diffusion at periods close to the evanescent region, but the phase of $\langle \eta \rangle$ is opposite in sign for the diffusive and nondiffusive cases at these periods. For $\nu = 200$ m^2 s^{-1} and $Pr = 2$ and 10, $\langle \eta \rangle$ is affected by Pr only at periods larger than about 10^4 s. The character of $\langle \eta \rangle$ versus period when $\nu = 50$ m^2 s^{-1} and $Pr = 2$, though not subject to the strong interference oscillations of the nondiffusive case, is clearly influenced by the upper limit of vertical integration. The peak in $|\langle \eta \rangle|$ at a period of about 10^4 s and the flattening of $|\langle \eta \rangle|$ versus period at larger periods in this case are consequences of the necessarily limited vertical integration. An eddy momentum diffusivity of 50 m^2 s^{-1} is not sufficiently large to completely eliminate the sensitivity of results to the range of vertical integration. Aside from the damping of interference oscillations, the main influence of diffusion on $\langle \eta \rangle$ is the reversal in sign of the phase.

SUMMARY OF RESULTS

The major results of the present study are conveniently summarized in Figures 17–19, which give the dependence on period of $|\langle \delta I \rangle / \langle \bar{I} \rangle|$, $|\langle \delta T_I \rangle / \langle \bar{T}_I \rangle|$, and $\langle \eta \rangle$, respectively, for

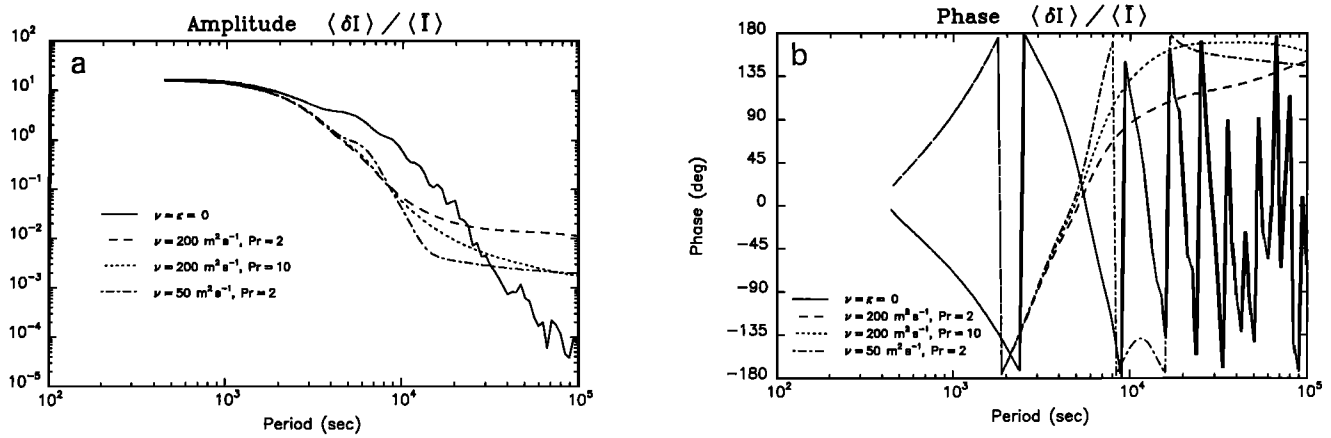

Fig. 12. (*a*) Amplitude and (*b*) phase of $\langle \delta I \rangle / \langle \bar{I} \rangle$ versus period for no eddy diffusion $\nu = \kappa = 0$ and for three cases with eddy diffusion, including the nominal case $\nu = 200$ m^2 s^{-1}, $Pr = 2$. The horizontal wavelength λ_x = 100 km.

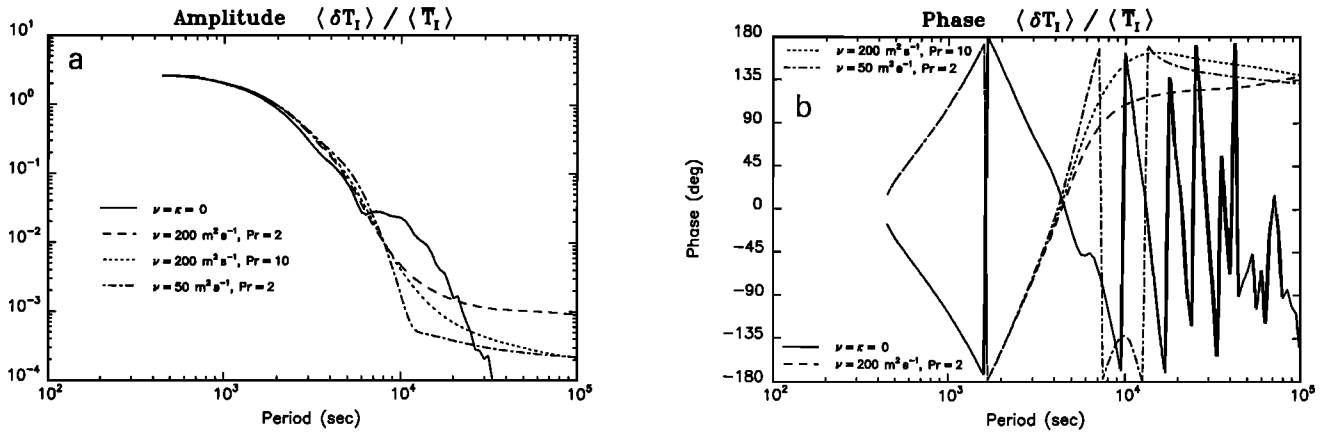

Fig. 14. Similar to Figure 12, but for the vertically integrated normalized temperature perturbation $\langle \delta T_I \rangle / \langle \bar{T}_I \rangle$.

λ_x = 100 km and for emission from a single level and an extended region both with and without eddy diffusion. The four different approximations all do a reasonable job of describing the normalized height integrated fluctuations in intensity and temperature and the height integrated Krassovsky's ratio at short gravity wave periods close to the evanescent region. At longer gravity wave periods, the approximation of emission from a single level with no eddy diffusion is not adequate for representing the ratios $\langle \delta I \rangle / \langle \bar{I} \rangle$, $\langle \delta T_I \rangle / \langle \bar{T}_I \rangle$, and $\langle \eta \rangle$. Taking account of emission from an extended layer, but with $\nu = \kappa = 0$, gives normalized height-integrated intensity and temperature fluctuations that are subject to interference maxima and minima at longer gravity wave periods due to the finite range of vertical integration. The interference-related structures in $\langle \delta I \rangle / \langle \bar{I} \rangle$ and $\langle \delta T_I \rangle / \langle \bar{T}_I \rangle$ make the ratio of these quantities, $\langle \eta \rangle$, particularly subject to large interference oscillations at long gravity wave periods. It is essential to account for both eddy diffusion and emission from an extended region to correctly predict $\langle \eta \rangle$ (and the other ratios), particularly at long gravity wave periods. For λ_x = 100 km, amplitudes of the vertically integrated Krassovsky's ratio are large (in excess of 5) at all gravity wave periods and in excess of 10 at periods greater than about 2 hours. The phase of $\langle \eta \rangle$ is between about 0 and $-\pi/4$ at short gravity wave periods, increasing to about 10° at a period of 10^5 s. Though not shown in this last set of figures, we have seen in Figure 15 that values of $|\langle \eta \rangle|$ less than 5 occur at gravity wave periods less than about 4×10^4 s for large horizontal wavelengths (λ_x = 1000 km).

Discussion and Concluding Remarks

The results presented here demonstrate the importance of including the effects of eddy momentum and thermal diffusivities in the gravity wave dynamics when calculating OH emission perturbations and related variables. Eddy diffusion mitigates interference effects associated with a finite range of vertical integration.

A comparison of the results of the present theory with observations of Krassovsky's ratio reported in the literature [*Hecht et al.*, 1987; *Sivjee et al.*, 1987; *Viereck and Deehr*, 1989] is presented in Figure 20. The values of $\langle \eta \rangle$ included in Figure 20 are inferred from OH(6,2) and OH(8,3) airglow observations obtained at different times and locations. The data are simply plotted together in Figure 20 as a function of period, and no attempt has been made to vary model parameters to best fit the observations. Figure 20 is intended to provide only a qualitative comparison of theory and data. The theoretical curves in the figure are for the nominal diffusivity parameters adopted in this paper and include effects of integration over the extended emission region. Figure 20 shows that it is reasonable to interpret the fluctuations in OH airglow at periods in excess of about 2 hours, as caused by vertically propagating gravity waves. The observed magnitudes of $\langle \eta \rangle$ are consistent with the theoretical predictions of $|\langle \eta \rangle|$ provided that the gravity waves have horizontal wavelengths of about 500–1000 km or more (Figure 20*a*). These wavelengths are consistent with the most energetic fluctuations in the horizontal wavenumber spectra derived from observations and theoretical considerations [see *Lilly*, 1983, and references therein].

The trend in the values of $|\langle \eta \rangle|$ inferred by *Viereck and Deehr* [1989] is for $|\langle \eta \rangle|$ to increase with period for periods greater than about 2 hours. Theory predicts a similar increase of $|\langle \eta \rangle|$ with period at periods between about 2 or 3

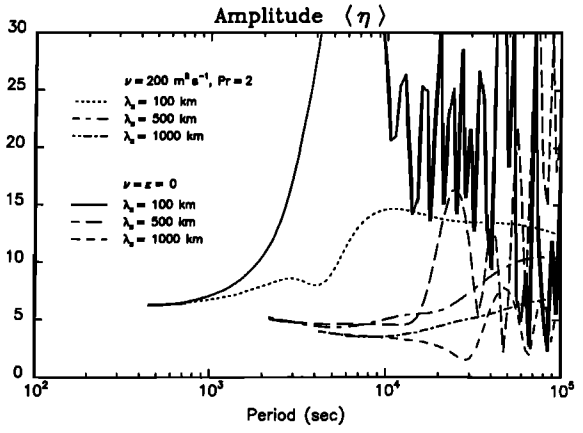

Fig. 15. Similar to Figure 11, but for the vertically integrated Krassovsky's ratio $\langle \eta \rangle$.

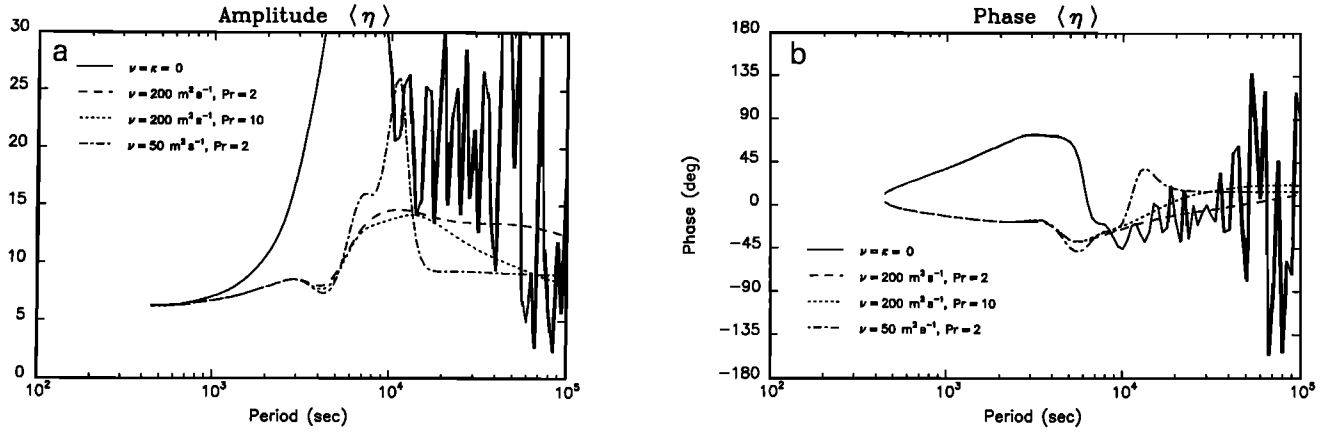

Fig. 16. Similar to Figure 12, but for the height-integrated Krassovsky's ratio $\langle \eta \rangle$.

hours and a day, depending on horizontal wavelength. Observations of the phase of $\langle \eta \rangle$ give values that are generally within ±45° of 0° in the period range of several hours to a day (Figure 20*b*). The theoretical curves of the phase of $\langle \eta \rangle$ versus period for λ_x = 500 and 1000 km give values in qualitative agreement with the observations. The slight undulations in the amplitude and phase of η between periods of ~1 and 3 × 10^4 s arise from very subtle differences between the rates of change of $\langle \delta I \rangle / \langle \bar{I} \rangle$ and $\langle \delta T_I \rangle / \langle \bar{T}_I \rangle$ (see, for example, Figures 11 and 13), and they may not be a robust result.

Previous attempts to compare theory and observations of $\langle \eta \rangle$ have used a variety of simplifications of the present theory, at times assuming emission from a single level or neglect of eddy diffusion. The results of the more complete theory presented in this paper and the comparison with observations stress the importance of applying the theory in its general form to interpret measurements of OH airglow fluctuations. Values of $\langle \eta \rangle$ are strongly dependent on the background state of the atmosphere, the period and horizontal wavelength of the perturbing gravity wave, the inclusion of eddy thermal and momentum diffusion and the specific values of the diffusivities, and integration over the vertical extent of the emission region. If future observations of fluctuations in the OH nightglow can identify the horizontal wavelengths of the gravity waves driving the fluctuations, then comparison of observed and predicted values of $\langle \eta \rangle$ over a range of periods may allow the inference of the eddy diffusivities in the emission region of the mesopause.

We have carried out calculations similar to those reported here for the acoustic wave regime. In general, the effects of eddy diffusion on acoustic wave properties (e.g., λ_v and the polarization factors (f_1, f_2, f_3) and the ratios $\langle \delta I \rangle / \langle \bar{I} \rangle$, $\langle \delta T_I \rangle / \langle \bar{T}_I \rangle$, and $\langle \eta \rangle$ at acoustic wave periods are small, at least for the horizontal wavelengths and eddy diffusion values considered here. The phase of $\langle \eta \rangle$ is sensitive to the inclusion of eddy diffusion at acoustic wave periods; the effect of nonzero ν and κ is to reverse the sign of the phase of $\langle \eta \rangle$, compared to the $\nu = \kappa = 0$ case, at acoustic periods.

There is evidence that the perhydroxyl reaction may be unimportant in the production of excited OH (OH*) [e.g., *Kaye*, 1988], or that it may be involved as a sink for OH* above v = 6 rather than as a source of OH* below v = 6 [*McDade and Llewellyn*, 1987]. Also, *Lopez-Moreno et al.* [1987] have reported that there is a different altitude distribution for each of the different vibrational levels of OH*. These considerations, and the inclusion of quenching effects, lie beyond the scope of this paper, but it is noted that future models may need to include them to properly describe the OH* emission characteristics.

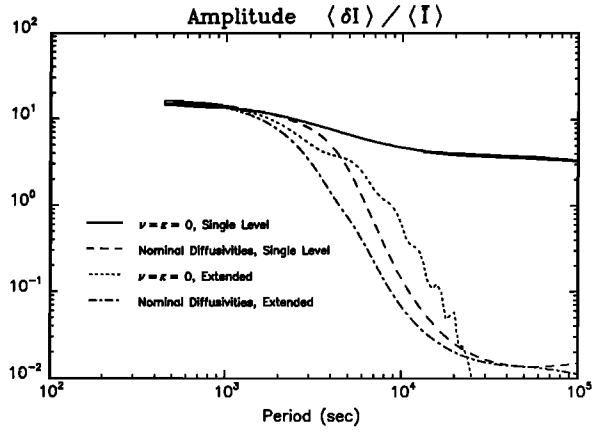

Fig. 17. Magnitude of the vertically-integrated normalized intensity fluctuation $\langle \delta I \rangle / \langle \bar{I} \rangle$ as a function of period for emission from a single level and from an extended region, both without eddy diffusion $\nu = \kappa = 0$ and with eddy diffusion given by the nominal diffusivity values ν = 200 m^2 s^{-1}, Pr = 2. The horizontal wavelength is 100 km.

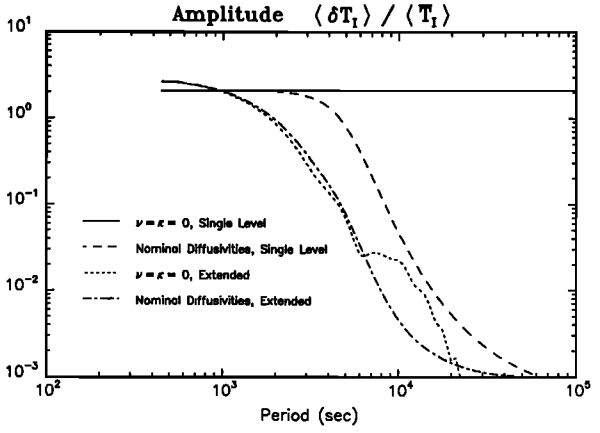

Fig. 18. Similar to Figure 17, but for $\langle \delta T_I \rangle / \langle \bar{T}_I \rangle$.

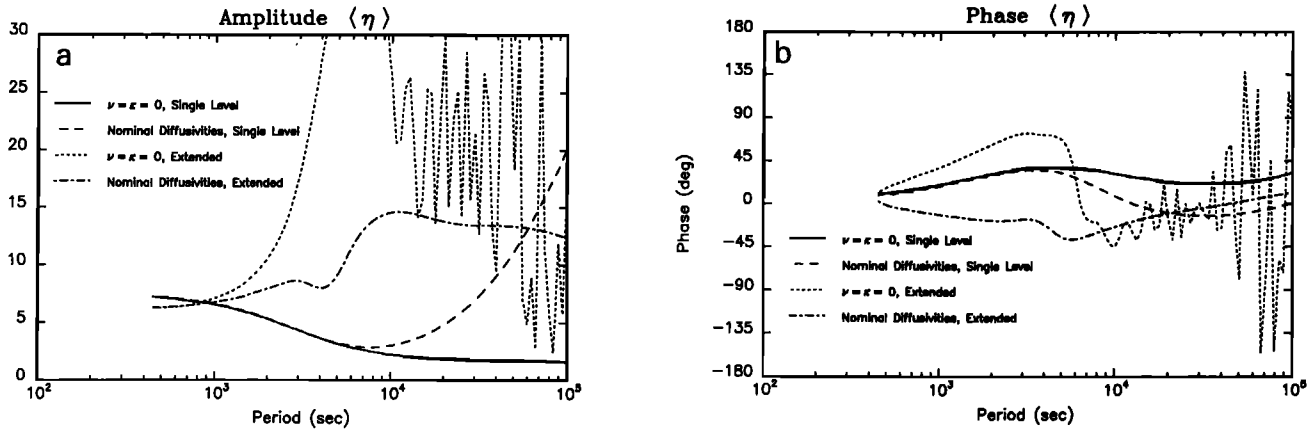

Fig. 19. Similar to Figure 17, but for the (*a*) amplitude and (*b*) phase of ⟨η⟩, the height-integrated Krassovsky's ratio.

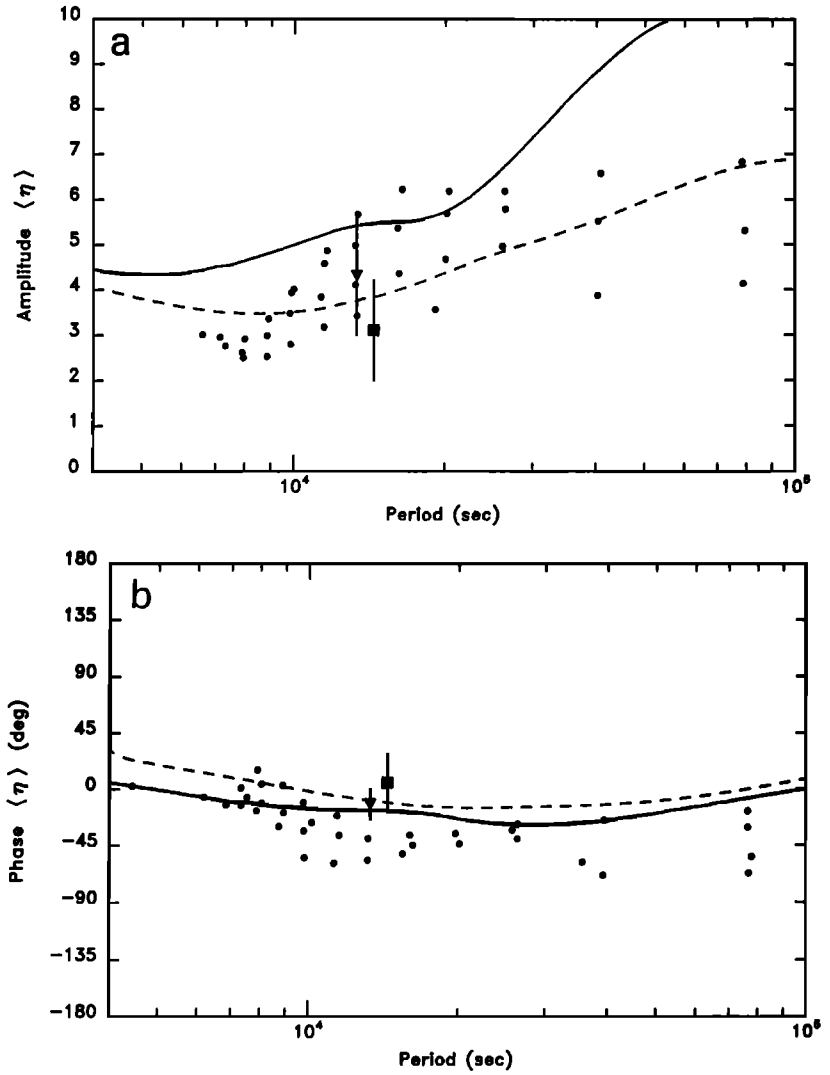

Fig. 20. Comparison of the (*a*) amplitude and (*b*) phase of Krassovsky's ratio ⟨η⟩ inferred from observations of OH(6, 2) and OH(8, 3) airglow with the theoretical predictions of this paper. The theoretical curves of ⟨η⟩ versus period are for the nominal diffusivity parameters and account for emission from an extended region (solid curve λ_x = 500 km, dashed curve λ_x = 1000 km). The solid circles represent values of ⟨η⟩ deduced from the airglow observations of *Viereck and Deehr* [1989], while the solid square and triangle and associated error bars indicate values of ⟨η⟩ inferred from the airglow measurements of *Hecht et al.* [1987] and *Sivjee et al.* [1987], respectively.

APPENDIX: DISPERSION AND POLARIZATION RELATIONS FOR PLANE ACOUSTIC-GRAVITY WAVES WITH EDDY DIFFUSION

Walterscheid et al. [1987] and *Schubert and Walterscheid* [1988] used the acoustic-gravity wave theory of *Hines* [1960] for an inviscid, nonthermally conducting atmosphere. *Hickey* [1988*a*, *b*] used the acoustic-gravity wave formulas of *Hickey and Cole* [1987] to study the effects of viscosity and thermal diffusivity on OH emission from a thin layer. The theory of *Hickey and Cole* [1987] models the effects of eddy kinematic viscosity and eddy thermal diffusivity as analogous to that of molecular kinematic viscosity and molecular thermal diffusivity. Here, we derive a theory for acoustic-gravity wave propagation in an atmosphere with eddy momentum and eddy thermal diffusivities. In particular, eddy thermal diffusion acts on potential temperature θ, a quantity which is conserved in the absence of diffusion.

The basic equations of continuity, momentum, energy, and state are

$$\frac{\partial \rho}{\partial t} + \nabla \cdot (\rho \mathbf{u}) = 0 \tag{A1}$$

$$\rho \frac{D\mathbf{u}}{Dt} = -\nabla p + \rho \mathbf{g} + \nabla \cdot (\rho \nu \nabla \mathbf{u}) \tag{A2}$$

$$\frac{D\theta}{Dt} = \frac{1}{\rho} \nabla \cdot (\rho \kappa \nabla \theta) \tag{A3}$$

$$p = \rho R T \tag{A4}$$

where ρ is density, $\mathbf{u}$ is velocity, p is pressure, T is temperature, $\mathbf{g}$ is the acceleration of gravity, ν is eddy momentum diffusivity, κ is eddy thermal diffusivity, R is the gas constant, t is time, D/Dt is the total derivative $D/Dt = (\partial/\partial t) + \mathbf{u} \cdot \nabla$. A perfect gas equation of state has been assumed and potential temperature is given by

$$\theta = T\left(\frac{1000 \text{ mbar}}{p}\right)^{R/c_p} \tag{A5}$$

where c_p is specific heat at constant pressure. The variables are written as the sum of basic state and perturbation quantities; e.g., $p = \bar{p} + \delta p$; $T = \bar{T} + \delta T$; $\rho = \bar{\rho} + \delta \rho$; $\theta = \bar{\theta} + \delta \theta$; and the equations for the perturbations are linearized. It is assumed that $\bar{T} = \text{const}$ and $\bar{u} = 0$, so that $\bar{\rho} = \rho_s \exp(-z/\bar{H})$ and $\bar{p} = p_s \exp(-z/\bar{H})$, where ρ_s and p_s are basic state surface ($z = 0$) density and pressure, respectively, z is altitude, and $\bar{H}$ is the basic state scale height, $\bar{H} = R\bar{T}/g$.

Potential temperature in the basic state is

$$\bar{\theta} = \bar{T}\left(\frac{1000 \text{ mbar}}{p_s}\right)^{R/c_p} \exp\left(\frac{zR}{c_p \bar{H}}\right) \tag{A6}$$

Perturbation quantities are written as

$$(\delta u, \delta v, \delta w) = \left(\frac{\omega}{k_x}\hat{u}', 0, \frac{\omega}{k_x}\hat{w}'\right) \cdot \exp(z/2\bar{H}) \exp[i(\omega t - k_x x - k_z z)] \tag{A7}$$

$$\delta p = p_s \hat{p}' \exp(-z/2\bar{H}) \exp[i(\omega t - k_x x - k_z z)] \tag{A8}$$

$$\delta \rho = \rho_s \hat{\rho}' \exp(-z/2\bar{H}) \exp[i(\omega t - k_x x - k_z z)] \tag{A9}$$

$$\delta T = \bar{T}\hat{T}' \exp(z/2\bar{H}) \exp[i(\omega t - k_x x - k_z z)] \tag{A10}$$

$$\delta \theta = \bar{\theta}_s \hat{\theta}' \exp(zR/\bar{H}c_p) \exp[i(\omega t - k_x x - k_z z)] \tag{A11}$$

where it has been assumed that all perturbation quantities are vertically propagating plane waves with complex height-dependent amplitudes, wave propagation occurs in the x-z plane, and the y component of perturbation velocity is zero. The surface value of the basic state potential temperature $\bar{\theta}_s$ is $\bar{T}(1000 \text{ mbar}/p_s)^{R/c_p}$. The plane wave has circular frequency ω, horizontal wavenumber k_x, and complex vertical wavenumber k_z.

The linearized equations for the perturbation quantities are

$$\hat{\rho}' = \hat{u}' + \hat{w}'(\delta - i\alpha) \tag{A12}$$

$$\beta \hat{u}' = \hat{p}' - \beta \chi_M \hat{u}'(i\delta\alpha - \delta^2 - 1) \tag{A13}$$

$$\beta \hat{w}' = \hat{p}'(\delta - i\alpha) + i\alpha \hat{p}' - \beta \chi_M \hat{w}'(i\delta\alpha - \delta^2 - 1) \tag{A14}$$

$$\hat{\theta}' + \frac{R\alpha}{ic_p}\hat{w}' = \hat{\theta}'\chi_H\left\{1 - i\alpha\left(\delta + \frac{iR\alpha}{c_p}\right) + \left(\delta + \frac{iR\alpha}{c_p}\right)^2\right\} + \frac{\hat{\rho}' R\alpha \chi_H}{c_p}\left\{\alpha + i\delta - \frac{R\alpha}{c_p}\right\} \tag{A15}$$

$$\hat{p}' = \hat{T}' + \hat{\rho}' \tag{A16}$$

$$\hat{\theta}' = -\frac{R}{c_p}\hat{p}' + \hat{T}' \tag{A17}$$

where

$$\alpha = \frac{1}{k_x \bar{H}}, \qquad \delta = \frac{k_z}{k_x} + \frac{i\alpha}{2} \tag{A18}$$

$$\beta = \omega^2/k_x^2 g\bar{H} \tag{A19}$$

$$\chi_H = ik_x^2\kappa/\omega, \qquad \chi_M = ik_x^2\nu/\omega \tag{A20}$$

Equations (A12)–(A17) are homogeneous, linear algebraic equations for the complex amplitudes of the perturbation variables. The dispersion relation for the waves follows from setting the determinant of the coefficient matrix to zero and solving for the roots of the resulting polynomial equation in δ. It is straightforward to first eliminate $\hat{\rho}'$ and $\hat{\theta}'$ from this system and reduce the equations to a set of four equations for the four unknowns $\hat{p}'$, $\hat{T}'$, $\hat{u}'$, and $\hat{w}'$. The 4×4 determinant that provides the dispersion relation has the following elements

First row

$$(-1, 1, 1, \delta - i\alpha)$$

Second row

$$\{1, 0, \beta[-1 + \chi_M(1 - i\alpha\delta + \delta^2)], 0\}$$

Third row

$$\left\{\frac{i\delta}{\alpha},\ 1,\ 0,\ \frac{i\beta}{\alpha}\left[-1+\chi_M(1-i\alpha\delta+\delta^2)\right]\right\}$$

Fourth row

$$\left\{-\frac{R}{c_p}+\frac{R\chi_H}{c_p}\left[1-\alpha^2+\left(\delta+\frac{iR\alpha}{c_p}\right)^2-2i\alpha\left(\delta+\frac{iR\alpha}{c_p}\right)\right],\right.$$
$$1-\chi_H\left[1-i\alpha\delta+\left(\delta+\frac{iR\alpha}{c_p}\right)^2\right.$$
$$\left.\left.-\frac{iR\alpha}{c_p}\left(\delta+\frac{iR\alpha}{c_p}\right)\right],\ 0,\ \frac{R\alpha}{ic_p}\right\}.$$

The dispersion relation is a sixth-order polynomial equation for δ.

The theory for the fluctuations in OH nightglow intensity requires the polarization relations

$$-i\hat{u}'+\hat{w}'\left(-i\frac{k_z}{k_x}+\frac{1}{2k_x\bar{H}}\right)=\frac{f_1}{\omega}\hat{T}' \tag{A21}$$

$$\hat{w}'=f_2\frac{k_x}{\omega}\hat{T}' \tag{A22}$$

$$\hat{\rho}'=f_3\hat{T}' \tag{A23}$$

It can be shown from (A12) through (A17) that

$$k_xf_2/\omega=\{(\alpha+i\delta)[1-\beta+\beta\chi_M(1+\delta^2-i\alpha\delta)]$$
$$-i\delta\}/\{i\delta(\delta-i\alpha)-[-i\beta+i\beta\chi_M(1+\delta^2-i\alpha\delta)$$
$$+i\delta(\delta-i\alpha)][1-\beta+\beta\chi_M(1-\delta^2-i\alpha\delta)]\} \tag{A24}$$

$$f_3=\frac{k_xf_2}{\omega}(\delta-i\alpha)-\frac{1+[(k_xf_2/\omega)(\delta-i\alpha)]}{1-\beta+\beta\chi_M(1+\delta^2-i\alpha\delta)} \tag{A25}$$

$$f_1=(f_2/\bar{H})-i\omega f_3 \tag{A26}$$

Acknowledgments. This work was supported by the Aerospace Sponsored Research Program (G.S. and R.L.W.), by NASA under contract NAS8-36639 (M.P.H.), and by NSF under grant ATM90-00216. We thank Michael McNab for carrying out the numerical calculations.

The Editor thanks D. Tarasick and P. Espy for their assistance in evaluating this paper.

REFERENCES

Hecht, J. H., R. L. Walterscheid, G. G. Sivjee, A. B. Christensen, and J. B. Pranke, Observations of wave-driven fluctuations of OH nightglow emission from Sondre Stromfjord, Greenland, *J. Geophys. Res.*, *92*, 6091–6099, 1987.

Hickey, M. P., Effects of eddy viscosity and thermal conduction and coriolis force in the dynamics of gravity wave driven fluctuations in the OH nightglow, *J. Geophys. Res.*, *93*, 4077–4088, 1988*a*.

Hickey, M. P., Wavelength dependence of eddy dissipation and coriolis force in the dynamics of gravity wave driven fluctuations in the OH nightglow, *J. Geophys. Res.*, *93*, 4089–4101, 1988*b*.

Hickey, M. P., and K. D. Cole, A quartic dispersion equation for internal gravity waves in the thermosphere, *J. Atmos. Terr. Phys.*, *49*, 889–899, 1987.

Hines, C. O., Internal gravity waves at ionospheric heights, *Can. J. Phys.*, *38*, 1441–1481, 1960.

Hines, C. O., and D. W. Tarasick, On the detection and utilization of gravity waves in airglow studies, *Planet. Space Sci.*, *35*, 851–866, 1987.

Kaye, J. A., On the possible role of the reaction $O + HO_2 \rightarrow OH + O_2$ in OH airglow, *J. Geophys. Res.*, *93*, 285–288, 1988.

Krassovsky, V. I., Infrasonic variations of OH emission in the upper atmosphere, *Ann. Geophys.*, *28*, 739–746, 1972.

Lilly, D. K., Stratified turbulence and the mesoscale variability of the atmosphere, *J. Atmos. Sci.*, *40*, 749–761, 1983.

Lopez-Moreno, J. J., R. Rodrigo, F. Moreno, M. Lopez-Puertas, and A. Molina, Altitude distribution of vibrationally excited states of atmospheric hydroxyl at levels $v = 2$ to $v = 7$, *Planet. Space Sci.*, *35*, 1029–1038, 1987.

McDade, I. C., and E. J. Llewellyn, Kinetic parameters related to sources and sinks of vibrationally excited OH in the nightglow, *J. Geophys. Res.*, *92*, 7643–7650, 1987.

Schubert, G., and R. L. Walterscheid, Wave-driven fluctuations in OH nightglow from an extended source region, *J. Geophys. Res.*, *93*, 9903–9915, 1988.

Sivjee, G. G., R. L. Walterscheid, J. H. Hecht, R. M. Hamwey, G. Schubert, and A. B. Christensen, Effects of atmospheric disturbances on polar mesopause airglow OH emissions, *J. Geophys. Res.*, *92*, 7651–7656, 1987.

Tarasick, D. W., and C. O. Hines, The observable effects of gravity waves on airglow emissions, *Planet. Space Sci.*, *38*, 1105–1119, 1990.

Viereck, R. A., and C. S. Deehr, On the interaction between gravity waves and the OH Meinel (6–2) and the O_2 atmospheric (0–1) bands in the polar night airglow, *J. Geophys. Res.*, *94*, 5397–5404, 1989.

Walterscheid, R. L., and G. Schubert, A dynamical-chemical model of tidally driven fluctuations in the OH nightglow, *J. Geophys. Res.*, *92*, 8775–8780, 1987.

Walterscheid, R. L., G. Schubert, and J. M. Straus, A dynamical-chemical model of wave-driven fluctuations in the OH nightglow, *J. Geophys. Res.*, *92*, 1241–1254, 1987.

Winick, J. R., Photochemical processes in the mesosphere and lower thermosphere, in *Solar-Terrestrial Physics*, edited by R. L. Carovillano and J. M. Forbes, pp. 677–732, D. Reidel, Hingham, Mass., 1983.

M. P. Hickey, FWG Associates, P.O. Box 12056, Huntsville, AL 35815-2056.

G. Schubert and R. L. Walterscheid, Space Sciences Laboratory, The Aerospace Corporation, Los Angeles, CA 90009.

(Received June 8, 1990;
revised February 19, 1991;
accepted February 21, 1991.)